



## Research Paper

# Hollow branched fiber hierarchical porous carbon as recyclable adsorbents and catalysts for efficient CO<sub>2</sub> capture and conversion

Ling Shi<sup>a</sup>, Ke-Yi Liao<sup>b</sup>, Yu-Hua Dong<sup>b</sup>, Yi-An Wang<sup>b</sup>, Yan Zhou<sup>a</sup>, Xiu-Guang Yi<sup>c</sup>,  
Ming-Shuai Sun<sup>a</sup>, Wei Hui<sup>a,b,\*</sup>, Duan-Jian Tao<sup>a,\*</sup>

<sup>a</sup> Key Laboratory of Fluorine and Silicon for Energy Materials and Chemistry of Ministry of Education, College of Chemistry and Chemical Engineering, Jiangxi Normal University, Nanchang 330022, China

<sup>b</sup> School of Life Science, Jinggangshan University, Ji'an 343009, China

<sup>c</sup> School of Chemistry and Chemical Engineering, Jinggangshan University, Ji'an 343009, China

## ARTICLE INFO

## Keywords:

Hollow fiber  
CO<sub>2</sub> capture  
CO<sub>2</sub> conversion  
Hierarchical porous carbon

## ABSTRACT

The promotion of carbon neutrality has been fueling the rapid growth of the new energy vehicle industry. However, this expansion inevitably brings about the devilish problem of waste disposal and environmental pollution. Melamine foam, as a typical sound insulation material for new energy vehicles, has also been considered a valuable organic precursor in recent years due to its high carbon and nitrogen content. In this study, we reused waste melamine foam through a simple carbonization-pyrolysis process, to obtain a series of hollow fiber hierarchical porous carbon materials (MFC) with different functions. Surprisingly, the MFC materials exhibit excellent CO<sub>2</sub> capture and conversion capability. For example, MFC-900 has a CO<sub>2</sub> capture capacity of 1.37 mmol g<sup>-1</sup> at 1 bar and 50 °C, which increases significantly to 5.05 mmol g<sup>-1</sup> at 1 bar and 0 °C. Additionally, the CO<sub>2</sub> selectivity of MFC-900 material is 285 at 50 °C, outperforming comparable hierarchical porous carbon materials. This superior performance is attributed to the unique hollow branched fiber structure and multiple types of basic centers of MFC materials. Furthermore, the MFCs demonstrate high catalytic efficiency, facilitating the conversion of CO<sub>2</sub> and epoxides into cyclic carbonates with yield of up to 99%. Therefore, based on the superior CO<sub>2</sub> capture and conversion performance of the MFC materials in this work, a new method of converting waste carbon resources into functional carbon is proposed for the field of carbon neutrality.

## 1. Introduction

The increased carbon dioxide (CO<sub>2</sub>) concentrations have been recognized as a major driver of climate change problems, including global warming, glaciers melting and ocean acidification. Obviously, these disasters will threaten human survival, and it is urgent to achieve carbon emission reduction under the strategy for sustainable development [1–3]. Carbon capture and utilization (CCU) is a technology that reduces CO<sub>2</sub> emissions by separating CO<sub>2</sub> from emission sources and converting it into high value-added chemical products through chemical methods, which is beneficial to both environment and economy [4–7]. One of the most important steps in the CCU is the selective capture and activation of CO<sub>2</sub>, which involve the use of adsorbents and catalysts, respectively. For adsorbents, high affinity, capacity, regeneration energy and gas selectivity are necessary to separate carbon dioxide from gas

mixtures. On the other hand, the catalysts must be characteristic of satisfactory activity, stability, selectivity and recyclability to promote chemical reactions between CO<sub>2</sub> and other substrates. However, most reported CO<sub>2</sub> capture and catalytic materials face difficulty generally, such as the low adsorption capacity and gas selectivity, the poor catalytic activity and stability, limiting the efficiency and sustainability of CCU [8]. Moreover, CCU strategy also encounters technical, economic, environmental and social obstacles in practical application, so it is necessary to find more efficient, cost-effective and sustainable CCU routes. Therefore, a groundbreaking CCU material toward excellent activity in terms of CO<sub>2</sub> capture capacity, conversion efficiency and low energy consumption for regeneration is particularly desirable for current research.

In recent years, CO<sub>2</sub> capture and conversion research have made corresponding progress in the CCU field. For CO<sub>2</sub> capture, various CO<sub>2</sub>

\* Corresponding author at: Key Laboratory of Fluorine and Silicon for Energy Materials and Chemistry of Ministry of Education, College of Chemistry and Chemical Engineering, Jiangxi Normal University, Nanchang 330022, China.

E-mail addresses: [huiwei@jxnu.edu.cn](mailto:huiwei@jxnu.edu.cn) (W. Hui), [djtao@jxnu.edu.cn](mailto:djtao@jxnu.edu.cn) (D.-J. Tao).

<https://doi.org/10.1016/j.susmat.2024.e00880>

Received 7 January 2024; Received in revised form 6 February 2024; Accepted 29 February 2024

Available online 2 March 2024

2214-9937/© 2024 Elsevier B.V. All rights reserved.

capture methods have been developed, including physical and chemical absorption, membrane separation and gas-solid adsorption [9–13]. Among them, amine-based CO<sub>2</sub> absorption system is a mature technology widely used in power plants and industries, but it has some disadvantages, such as high energy consumption, equipment corrosion, and environmental problems during post-treatment [9,14,15]. Membrane separation has the advantages of uninterrupted operation, minimal energy consumption and compact equipment configuration, but has not yet been fully developed and is challenging in terms of membrane selectivity, permeability, mechanical strength, etc. [10,16] Fortunately, the porous materials are expected to be promising CO<sub>2</sub> adsorbents, as they could achieve the goal of high CO<sub>2</sub> capture capacity, high CO<sub>2</sub> selectivity and low energy consumption in regeneration [17–21]. Moreover, CO<sub>2</sub> utilization is another important consideration for CCU, which could convert spent carbon into working carbon, following the circular principle of near-zero emission [6]. However, the CO<sub>2</sub> conversion process is certainly difficult, because CO<sub>2</sub> has been proven to be a thermodynamically stable and kinetically inert molecule, with a high binding energy of 750 kJ mol<sup>-1</sup> (C=O bond) and a high energy gap between HOMO and LUMO of 13.7 eV [22,23]. This means that the one-electron reduction of CO<sub>2</sub> is subject to very high negative redox potential and requires external energy support in the form of heat, electricity, or radiation as well as highly reactive substrates such as epoxides, amines, or hydrogen for the reaction [24,25]. Therefore, suitable catalysts are needed to overcome the kinetic barrier and improve the selectivity and efficiency of the reaction. Heteroatom-doped porous carbon is one of the potential catalysts, as it can activate CO<sub>2</sub> through electron transfer to the antibonding orbitals of CO<sub>2</sub> molecules, thereby lowering the reaction barrier.

Based on the above progress, some researchers have noticed the development of advanced carbon materials, which realize the entire CCU process in one step through the rational design of porous materials with active sites [26–28]. For example, it is shown that employing melamine as a precursor can effectively increase the amount of heteroatoms doped in biomass carbon materials, thus significantly enhancing the CO<sub>2</sub> capture and/or catalytic performance [29]. However, it is worth noting that most of the reported ones have complicated preparation methods and unsatisfactory performance. Tao et al. prepared nitrogen-doped porous carbon materials by pyrolyzing N-rich biomass materials, following economic and environmental principles [30]. Tea waste-derived carbon materials exhibited excellent CO<sub>2</sub> capture and conversion capabilities. Similarly, researchers also used waste products from human activities, such as coffee grounds and shrimp shells, to produce porous carbon materials [31–33]. These materials have exceptional features, such as high porosity, specific surface area, catalytic activity, and thermal stability, making them suitable for CO<sub>2</sub> capture and conversion [8,30]. The rapid increase in the number of new energy vehicles poses new challenges to the disposal of end-of-life vehicles in the future. Obviously, upcycling strategies will reuse parts of end-of-life vehicles, thereby reducing resource waste and environmental pollution. Melamine foam, a common material for vehicle insulation and noise reduction, has been found to contain significant amounts of carbon and nitrogen [34,35], and would be expected to be a potential candidate for CCU targets.

Herein, we developed a simple technique to transform sound-absorbing materials from new energy vehicles into hollow branched fiber hierarchical porous carbon (MFC) materials. These MFC materials can efficiently capture CO<sub>2</sub> with high capacity at 0/25/50 °C. Compared to similar carbon materials, these MFC materials have multiple basic centers and unique hollow branched fiber, which gives them significant advantage in CO<sub>2</sub> capture and activation. To verify the application potential of MFC materials in CO<sub>2</sub> conversion, we evaluated their catalytic performance in the cycloaddition reaction of CO<sub>2</sub> and epoxides. The results showed that MFC materials could effectively catalyze the reaction to prepare cyclic carbonates with yields up to 99%, thereby demonstrating their potential as CO<sub>2</sub> conversion catalysts. Moreover, we

investigated the chemical interaction of MFC materials on CO<sub>2</sub> and demonstrated their advantages in practical applications.

## 2. Experimental

### 2.1. Chemicals

Melamine foam (MF) were purchased from the Ledian flagship store on the Alibaba online platform. Tetrabutylammonium bromide (TBAB), epichlorohydrin (99 wt%), styrene oxide (SO, 98 wt%) and glycidyl vinyl ether (99 wt%) were purchased Shanghai Adamas Reagent Co. Ltd. *Tert*-Butyl glycidyl ether (96 wt%), glycidyl phenyl ether (99 wt%), 1,2-epoxyhexane (96 wt%) were purchased from Shanghai Macklin Biochemical Co. Ltd. CO<sub>2</sub> gas (99.99%) and N<sub>2</sub> gas (99.99%) were obtained from Nanchang Huasheng Gas Co. Ltd. He gas (99.99%) was obtained from Nanchang East China Special Co. Ltd. All reagents were used as received without further purification.

### 2.2. Synthesis of MFC materials

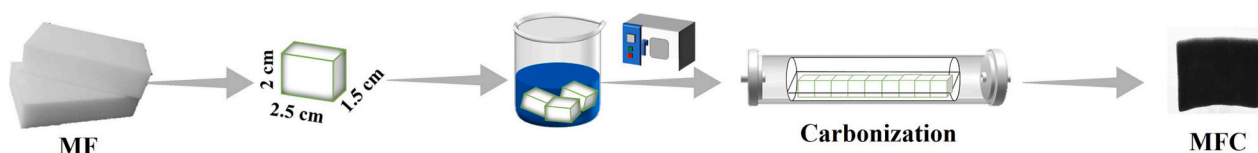
In Scheme 1, the synthesis of MFC materials is achieved through high-temperature carbonization. First, a MF was immersed in absolute ethanol and sonicated for 1 h. The clean MF was placed in a vacuum oven overnight to obtain dry MF, and then cut it into pieces (1.5 × 2 × 2.5 cm). Subsequently, these small pieces of MF were transferred to a tube furnace under nitrogen atmosphere for carbonization. The temperature program of the tube furnace is shown in Scheme S1. After cooling to room temperature, a black sponge-like solid was obtained, designated as MFC-X, where X is the carbonization temperature.

### 2.3. Characterizations of MFC materials

The samples were dried at 150 °C or degassed at 200 °C before characterization. The X-ray diffraction (XRD) patterns of the samples were obtained on an X'Pert powder diffractometer with a Cu K $\alpha$  radiation source of 40 kV and 40 mA at a scan rate of 5° min<sup>-1</sup> and a scanning angle of 10–80°. Brunauer-Emmett-Teller (BET) data for the samples were collected by N<sub>2</sub> adsorption-desorption analysis on a Micromeritics Tristar II 3020 instrument at -196 °C. The morphological characteristics of the samples were characterized by scanning electron microscope (SEM) on a HITACHI S-3400N instrument at an acceleration voltage of 5 kV. The surface valence states of the samples were analyzed by X-ray photoelectron spectroscopy (XPS) on an AXIS Ultra DLD instrument produced by KRATOS Analytical Co. Ltd., and the binding energy was corrected by the C1s peak of C–C at 284.8 eV. The Fourier-transformed infrared spectral (FT-IR) data of the samples were collected on a Spectrum One spectrometer. The Raman test of the samples were measured using a LabRAM HR spectrometer with a laser wavelength of 632 nm and a spectral resolution of 1.5 cm<sup>-1</sup>. An EA3000 elemental analyzer was used to determine the elemental composition of the samples. The basic sites of the samples were determined by temperature-programmed desorption (CO<sub>2</sub>-TPD) on a Micromeritics Autochem II 2920 instrument. The programmed temperature range was 25–800 °C, and the heating rate was 10 °C min<sup>-1</sup>.

### 2.4. CO<sub>2</sub> cycloaddition

In a typical CO<sub>2</sub> chemical fixation reaction carried out by the MFC catalysts, SO and CO<sub>2</sub> are used as reaction substrates. Firstly, 0.24 g SO was put into a high-pressure reactor, followed by 10 mg MFC and 10 mg TBAB in sequence. Then, the high-pressure reactor was closed and vacuumed for 1 h. Finally, open the air inlet valve of the device and fill it with CO<sub>2</sub> to keep the internal pressure of the reactor constant at 6 bar. Subsequently, the device was maintained at 110 °C for 2 h along with stirring at 800 rpm. For qualitative and quantitative analysis of reaction products, the products were determined by GC-MS, and the yield and



**Scheme 1.** The synthesis of MFC materials through high-temperature carbonization.

selectivity of the products were assessed by GC.

### 3. Results and discussion

#### 3.1. Structural characterizations

In this work, we successfully prepared reusable MFC materials from waste foams using an economical and simple strategy. Through SEM and TEM, the surface morphology and structural characteristics was observed for MFC materials at the microscopic level (see Figs. 1 and S1). The SEM images show that MFC-800, MFC-900, and MFC-1000 have branched fibers with rough surfaces, which form interconnected three-dimensional frameworks with rich pore structures and many pores with a size of several microns. Besides, Fig. 1b also shows the hollow fiber structure in the MFC-900 materials. The TEM images reconfirm the porous structural and hollow characteristics of the MFC-900 material. The high-resolution TEM images in Fig. 1e showed that MFC-900 has a richer porous structure than the other two materials, and its branched fibers exhibit thin interiors and thick edges, indicating hollow features inside. The formation of these unique structures can be attributed to the pyrocondensation of MFC materials during the carbonization process. MF units gradually transform into structures containing carbon in the form of amino groups and other functional groups. Moreover, this process typically releases large amounts of gaseous substances, creating additional porous structures in the frameworks [19]. The framework nodes, which are consisted of spherical triangles, enhance the overall stability of the frame by reducing stresses. The temperature program of the carbonization process also influenced the structural features of the MFC materials, as the high-temperature carbonization process triggers complex carbonization reactions, and the formation of the porous frameworks is affected by minor system changes, such as temperature and heating rate.

The porous properties of MFC materials were quantitatively analyzed and compared by low-temperature  $N_2$  adsorption-desorption tests. The  $N_2$  adsorption-desorption isotherms and calculated texture features are summarized in Fig. 2, Fig. S2, Table 1, and Table S1. The MFC materials have micro- and macropores, which were determined by the volume of adsorption at relative pressures of  $0 < P/P_0 < 0.1$  and  $0.9 < P/P_0 < 1$ , respectively [27,36]. Fig. 2b shows the NLDFT curves of localized micro-

and mesopores of the MFC materials. The width of the micro-mesopores of the MFC materials are concentrated in the range of 1.8 to 3.6 nm. Furthermore, the NLDFT pore size distribution of MFC-900 material shows that it has hierarchical pore properties (see Fig. 2c). The hysteresis loops of  $N_2$  adsorption-desorption isotherms indicate the presence of mesopores in MFC materials at  $0.1 < P/P_0 < 0.9$  [37]. Therefore, the MFC materials have hierarchical porous structures. Apparently, the carbonization temperature affects the specific surface area, pore volume, and pore diameter of the MFC materials. As the carbonization temperature increases from 800 °C to 1000 °C, the specific surface area and pore volume increase, while the pore diameter decreases. This result suggests that selecting the appropriate carbonization temperature is an essential step in preparation of carbon-based products. Fig. S2 depicts the effect of heating rate ( $4\text{--}10\text{ }^\circ\text{C min}^{-1}$ ) on the surface area of the MFC-900 material. When the heating rate is  $6\text{ }^\circ\text{C min}^{-1}$ , and then decreases with further increase in the heating rate. This is because the heating rate influences the carbonization and graphitization processes of MF. High heating rate may cause the framework of the materials to collapse, resulting in a smaller specific surface area.

#### 3.2. Texture properties of MFC materials

Fig. 3 and Fig. S3 show the XRD and Raman patterns of the MFC materials. Each sample displays broad diffraction peak (002) centered at  $2\theta = 24.1^\circ$ , which is common for carbonaceous materials [30]. The broad peaks of MFC materials indicate the presence of amorphous carbons, which are thermodynamically metastable and lack the regular arrangement of the crystal structure. The XRD patterns of the MFC materials also show characteristic peaks related to crystal plane diffraction (100) in the  $43.3^\circ$  region [37]. This result was expected, because the carbonization process at relatively high temperatures does not fully graphitize the MF. However, an increasing gradient in carbonization temperatures enhances the degree of graphitization in MFC material. For example, the MFC-900 material has a higher diffraction peak intensity than the MFC-800 material, indicating a higher level of graphitization. This means that the carbonization at suitable temperature promotes the formation of graphite-like structures, which enhance the gas capture and thermal stability of MFC materials. Moreover, the carbonized MFC materials do not show any other

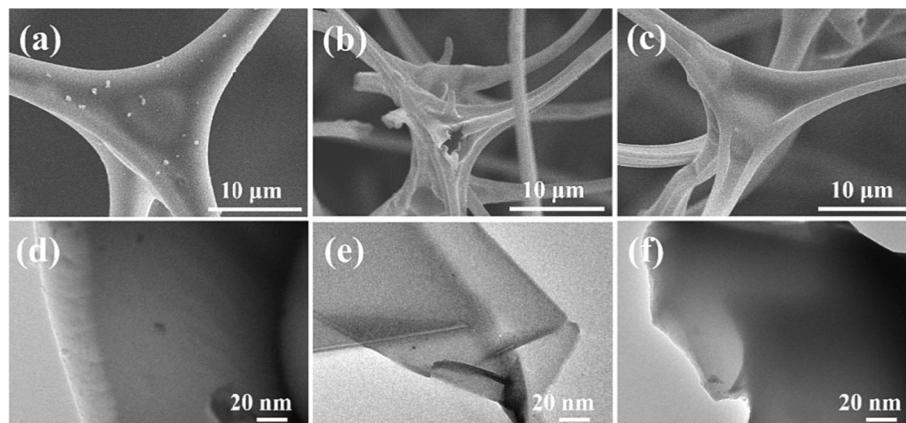


**Fig. 1.** SEM images of (a) MFC-800, (b) MFC-900 and (b) MFC-1000 samples, TEM images of (d) MFC-800, (e) MFC-900 and (f) MFC-1000 samples.

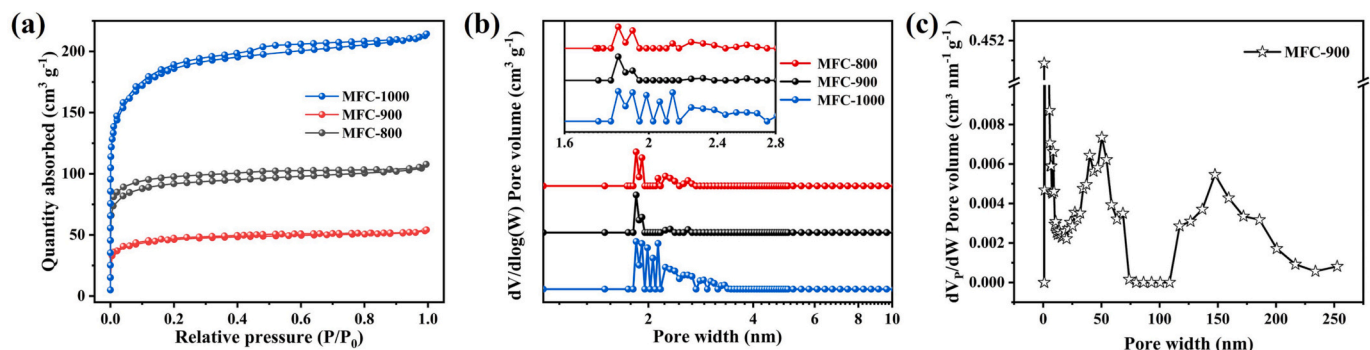


Fig. 2. (a) The  $N_2$  adsorption-desorption isotherms, (b) pore width curves of MFC-800, MFC-900 and MFC-1000 samples, (c) NLDFT pore width curves of MFC-900 sample.

Table 1

The structural features and  $CO_2$  capture capacities of MFC samples.

samples	$S_{BET}$ ( $m^2 g^{-1}$ )	$V_p$ ( $cm^3 g^{-1}$ )	$D_{ave}$ (nm)	Elemental analysis (wt%)				$CO_2$ uptake ( $mmol g^{-1}$ )		
				C	H	N	$O_{cal}$	0 °C	25 °C	50 °C
MFC-800	152	0.03	3.48	56.6	2.4	18.4	22.6	2.31	1.97	0.97
MFC-900	292	0.11	2.59	61.3	2.5	12.5	23.7	5.05	3.25	1.37
MFC-1000	692	0.21	2.30	69.8	3.1	6.5	20.6	4.26	2.19	1.20

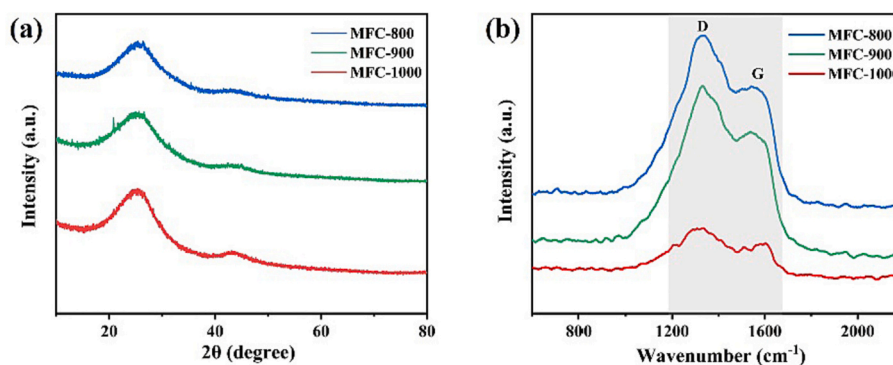


Fig. 3. (a) XRD patterns, (b) Raman spectra of MFC samples.

prominent peaks in their XRD patterns, indicating that they are free of impurities or crystallized carbon.

Raman spectral analysis can be used to determine the amorphous structure of MFC materials and collect the molecular rotational and vibrational energies of the molecules. Fig. 3b and Fig. S3b shows the peaks assigned to the D and G bands in MFC materials, which attribute to the stretching of the structurally defective C—C bonds on the graphite plane and the disordered  $sp^2$  hybridized carbon, respectively [38]. The degree of graphitization in MFC materials can be estimated by the ratio of D-band intensity ( $I_D$ ) to G-band intensity ( $I_G$ ). A lower  $I_D/I_G$  ratio indicates a higher degree of graphitization in the materials [39]. For example, the  $I_D/I_G$  ratios of MFC-900 and MFC-1000 materials are 1.24 and 1.16, respectively, while the  $I_D/I_G$  ratio of MFC-800 material is 1.27. This suggests that the MFC-800 material has a lower degree of graphitization due to its lower heat treatment temperature, which is insufficient to induce a pronounced graphitization. On the other hand, the MFC-1000 material has a higher degree of graphitization due to its high-temperature condition of 1000 °C, which shows a more pronounced difference compared to the MFC-800 and MFC-900 materials. The  $I_D/I_G$  ratios of MFC materials depend on the carbonization temperature. The carbonization of the carbon materials increases with the temperature, as evidenced by the decrease in the  $I_D/I_G$  ratios.

Furthermore, some studies have shown that the degree of graphitization plays a complementary role in  $CO_2$  capture by porous carbon materials [40,41]. Based on this, it can be inferred that the MFC materials with higher degree of graphitization might exhibit better  $CO_2$  capture performance at suitable specific surface areas and heteroatom contents.

### 3.3. $CO_2$ capture analysis of MFC materials

The  $CO_2$  capture capacities of the MFC materials were measured with the  $CO_2$  absorption isotherms at 0 °C and 1 bar (see Fig. 4a). The chemical and physical adsorption capabilities of  $CO_2$  in MFC materials were analyzed through iterative fitting using the empirical formula (see section S1.3 of the Supporting Information) [42]. This analysis aims to explore the interaction between different MFC materials and  $CO_2$  molecules. The fitted curves are displayed in Figs. 4b-d, and the estimated parameters are detailed in Table S2. The goodness-of-fit ( $R^2$ ) values between fitted curves and experimental data exceeds 0.99, indicating a good correlation. Furthermore, the roles of chemical and physical adsorption in the  $CO_2$  capture capacity of MFC materials were also speculated (see Figs. 4b-4d). It was observed that chemical adsorption appeared to play a significant role in the relative pressure range of 0–0.15 bar. For the MFC-800 and MFC-900 materials, the chemical

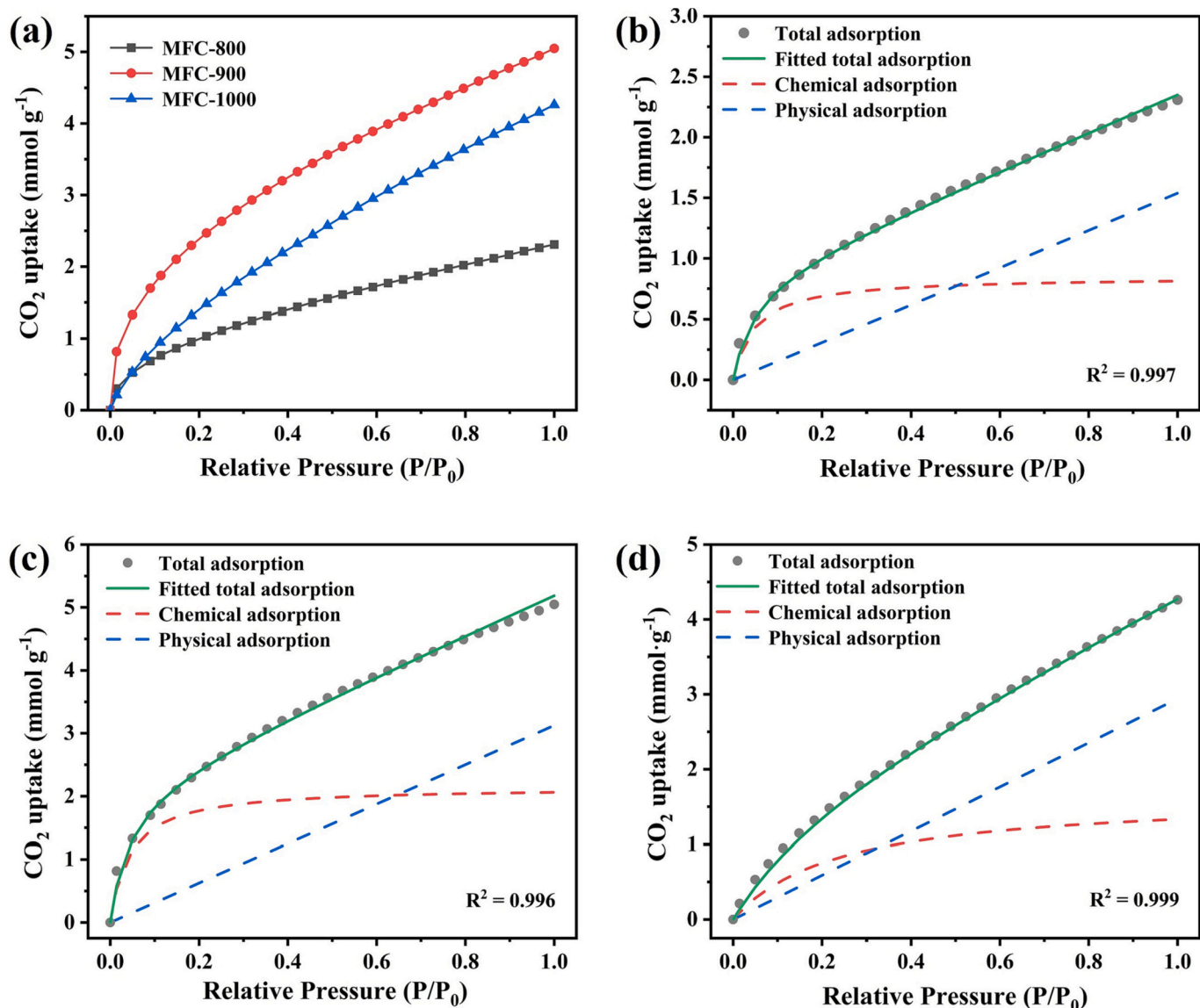


Fig. 4. (a) CO<sub>2</sub> capture isotherms of MFC-800, MFC-900 and MFC-1000 samples at 1 bar 0 °C, the fitted total, chemical and physical adsorption curves of CO<sub>2</sub> on (b) MFC-800, (c) MFC-900 and (d) MFC-1000 samples.

adsorption capacities seemingly remain constant over the relative pressure range of 0.15–1.0 bar, while the physical adsorption capacities increase linearly with the CO<sub>2</sub> partial pressure. Meanwhile, the isosteric heat ( $Q_{st}$ ) results showed that the  $Q_{st}$  values of MFC-900 material decreased overall with the increase of quantity adsorbed (see Fig. S5). Interestingly, it was found that in the range of 0–1.91 mmol g<sup>-1</sup> for CO<sub>2</sub> quantity adsorbed, the  $Q_{st}$  values of MFC-900 material were above 40 kJ mol<sup>-1</sup>, which implied that strong interaction between MFC-900 material and CO<sub>2</sub> molecules at this stage [43]. The above findings provided the scientific basis for analyzing and understanding the contribution of chemical and physical adsorption of MFC materials in the CO<sub>2</sub> capture process. Under the same operating conditions, MFC-900 has the highest CO<sub>2</sub> capture capacity (5.05 mmol g<sup>-1</sup>) among tested MFC materials and has the steepest slope of the chemical adsorption curve, indicating a strong affinity for CO<sub>2</sub>. This could be attributed to the high nitrogen content of MFC-900, which enhances the specific adsorption of CO<sub>2</sub> by the porous frameworks and the surface functional groups of MFC materials. The low adsorption capacity of MFC-1000, which has the lowest nitrogen content as shown in Table 1 and Table S3, and the gentle slope of its chemical adsorption curve support this hypothesis. However,

despite its rich nitrogen content, MFC-800 has a lower CO<sub>2</sub> capture capacity than MFC-900, implying the influence of another factor, which will be discussed later. The heating rate also affects the CO<sub>2</sub> capture performance of the MFC materials prepared with different heating rates, as shown in Fig. S4. The MFC-900 sample heated at 8 °C min<sup>-1</sup> has the optimal CO<sub>2</sub> capture performance under the same capture conditions.

The flue gas produced post-combustion has a temperature above 50 °C and a pressure around 1 bar. The choice of adsorbent is crucial for the efficiency of the CO<sub>2</sub> capture process. Adsorbent materials that can capture CO<sub>2</sub> at high temperatures are suitable for post-combustion capture. These materials should be cost-effective, stable, and have rapid adsorption and desorption cycles. The adsorption isotherms of the MFC materials were measured at 50 °C to evaluate their potential for CO<sub>2</sub> capture at high temperatures (see Fig. 5a). Obviously, the CO<sub>2</sub> capacities of MFC materials follow the order: MFC-900 > MFC-800 > MFC-1000. The MFC-900 material has a significantly higher capacity (1.37 mmol g<sup>-1</sup>) than the other two MFC materials, which can be attributed to its hollow carbon layers and the surface dispersion of more nitrogen species with good affinity for CO<sub>2</sub>. FT-IR was used to investigate the interaction between CO<sub>2</sub> and the MFC materials, different CO<sub>2</sub>

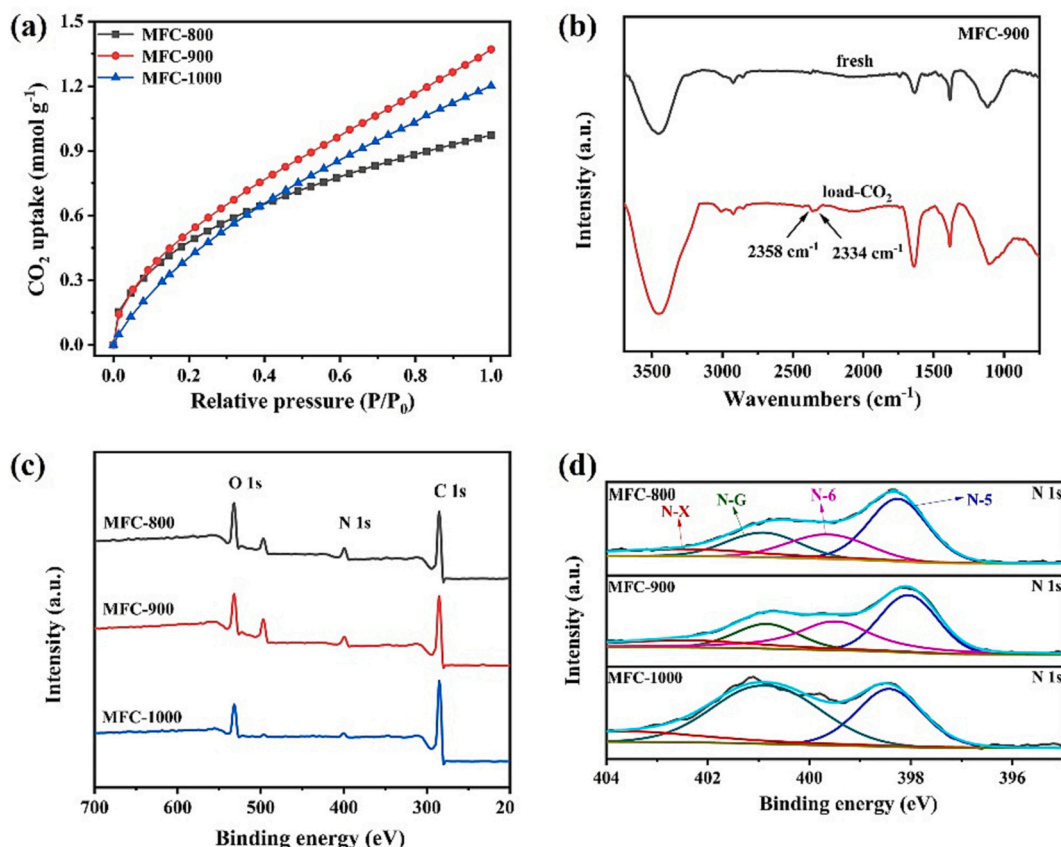


Fig. 5. (a) CO<sub>2</sub> capture isotherms of MFC-800, MFC-900 and MFC-1000 samples at 1 bar 50 °C, (b) FT-IR spectra of fresh and load-CO<sub>2</sub> MFC-900, (c) XPS full spectra and (d) N 1s spectra of MFC-800, MFC-900 and MFC-1000 samples.

adsorption modes on the material surface produce double peaks in the wavenumber range of 2330–2365 cm<sup>-1</sup> [44]. Saturated adsorption of pure CO<sub>2</sub> was performed on the typical MFC-900 material and tested under ambient conditions using FT-IR (see Fig. 5b). The load-CO<sub>2</sub> of the MFC-900 material showed red-shifted characteristic peaks at 2334 and 2360 cm<sup>-1</sup>, which indicate the interaction of CO<sub>2</sub> with the MFC materials, and confirm the fitting analysis results of the previous CO<sub>2</sub> uptake curves. MFC-900 was also compared to some CO<sub>2</sub> adsorbents reported in the literature and the results are summarized in Table 2. Overall, MFC-900 has a higher CO<sub>2</sub> capture capacity than many porous materials.

The XPS analysis confirms the impacts of nitrogen species present in the MFC materials for CO<sub>2</sub> capture, as shown in Fig. 5c and Fig. 5d. Clearly, Fig. 5c exhibits the C, N, and O signal peaks on the surfaces of MFC materials, and Table S3 summarizes the relative content of these

Table 2

Comparison of the CO<sub>2</sub> uptake capacity of MFC-900 with some other adsorbents at 1 bar.

Entry	Adsorbents	Temperature (°C)	CO <sub>2</sub> (bar)	CO <sub>2</sub> uptake (mmol g <sup>-1</sup> )	Ref.
1	PBC-700-800	0	1	4.53	[12]
	PBC-700-800	25	1	3.36	
2	SG-C	25	1	1.51	[45]
	SG-CN(2)	25	1	3.34	
3	M_800	0	1	3.90	[46]
4	HF-N-char	30	1	1.77	[47]
5	PN-3-K <sub>2</sub> CO <sub>3</sub>	30	1	2.26	[20]
6	CG600-1	0	1	4.54	[48]
		25	1	3.45	
7	MFC-900	0	1	5.05	This work
		25	1	3.25	
		50	1	1.37	

Table 3

Evaluate the catalytic activity of MFC catalysts for CO<sub>2</sub> and SO<sup>a</sup>.

Entry	catalyst	CO <sub>2</sub> pressure (bar)	Selectivity (%)	Yield (%)
1	MFC-900	4	99%	62%
2	MFC-900	5	99%	83%
3	MFC-900	6	99%	97%
4	MFC-800	6	99%	42%
5	MFC-1000	6	99%	64%
6 <sup>b</sup>	MFC-900	6	99%	33%
7	none	–	–	–

<sup>a</sup> Reaction condition: SO (2 mmol), catalyst (20 mg), TBAB (20 mg), 110 °C, 2 h.

<sup>b</sup> Reaction condition: SO (2 mmol), TBAB (20 mg), 110 °C, 2 h.

three elements. Fig. 5d displays the N 1s spectra of the MFC materials, which are deconvoluted into four peaks corresponding to pyridinic N (N-6), pyrrolic nitrogen (N-5), graphitic N (N-G), and pyridinic-N-oxide (N-X) [8]. Table S2 reports the relative nitrogen species content of MFC materials. As shown in Table S4, with the carbonization temperature rising, the percentage of N-G species increases, while the percentage of N-6/N-5 species decreases. The results imply that higher carbonization temperatures are beneficial to the formation of N-G species on MFC materials. The CO<sub>2</sub> capture by MFC materials involves the chemical adsorption dominated by N species and the physical adsorption caused by the well-developed pore structures. The N-G species and N-5 species have synergistic effect that improves the CO<sub>2</sub> capture capacity of the material. Furthermore, N-G species are not detrimental to CO<sub>2</sub> capture. The content of N-6/N-5 species in MFC-800 and MFC-900 materials is comparable, but the N-G species content in MFC-900 is 1.45 times that of MFC-800. Therefore, MFC-900 has a 1.41 times higher CO<sub>2</sub> capture

capacity than MFC-800 at 1 bar 50 °C.

Additionally, CO<sub>2</sub>-TPD was performed to determine the basicity of the MFC-900 material. It is generally believed that CO<sub>2</sub> adsorbed on weakly basic sites desorbs at low temperatures, while CO<sub>2</sub> adsorbed on strong basic sites desorbs at high temperatures [8]. The CO<sub>2</sub>-TPD profile of the MFC-900 material and the desorption peaks deconvoluted by the Lorentz model are shown in Fig. 6. It can be seen that the MFC-900 material has a weak CO<sub>2</sub> desorption peak at around 126 °C, indicating that the material contains weakly basic sites. Therefore, based on the above phenomenon, it can be inferred that this desorption peak is generated by weak chemical adsorption and physical adsorption of CO<sub>2</sub> on the framework. Besides, a desorption peak with a broad profile and strong signal is observed near 247 °C, which can be attributed to the presence of medium-strong basic sites in the MFC-900 material. This feature is conducive to enhancing the CO<sub>2</sub> capture capability of the MFC-900 material. Especially, the desorption peak centered at 627 °C represents that this peak may be related to the strongly chemisorbed CO<sub>2</sub>. In order to study this CO<sub>2</sub>-TPD profiles, the Lorentz mathematical model was used to evaluate the desorption peaks. The colored portion of Fig. 6 shows three different desorption peaks centered at 126 °C, 247 °C and 627 °C. This means that the hollow hierarchical porous framework of the MFC-900 material contains multiple types of basic centers with different strengths, which is consistent with the results of the FT-IR and XPS analyses. Overall, due to the structural properties of MFC-900 and the promotion of abundant nitrogen species, the kind of basic centers are really rich, which is positive to the high-selectivity and high-capacity CO<sub>2</sub> capture under higher temperature conditions.

The CO<sub>2</sub> selective capture performance of the synthesized MFC materials was tested by measuring their N<sub>2</sub> adsorption capacities. Figs. 7a-c and Fig. S6 show the N<sub>2</sub> adsorption isotherms of the MFC materials at 0 °C, 25 °C and 50 °C, respectively. The BET data indicates that the MFC materials interact weakly with N<sub>2</sub>, as the N<sub>2</sub> adsorption capacities increase approximately linearly with pressure. As a result, the MFC materials adsorb much less N<sub>2</sub> than CO<sub>2</sub>. For instance, MFC-900 adsorbs only 0.01 mmol g<sup>-1</sup> of N<sub>2</sub> at 0 °C and 0.85 bar. This demonstrated the potential of the MFC materials to selectively capture CO<sub>2</sub> from the combustion products of fossil fuels, which are also known to contain high concentrations of N<sub>2</sub>.

Based on the CO<sub>2</sub> and N<sub>2</sub> adsorption capacities, the CO<sub>2</sub>/N<sub>2</sub> selectivity of the synthesized MFC materials was predicted by using the ideal adsorbed solution theory (IAST), with the results shown in Figs. 7d-f [49]. Among the three MFC materials, MFC-900 obviously has the highest CO<sub>2</sub>/N<sub>2</sub> selectivity at 50 °C (IAST up to 285). This is because

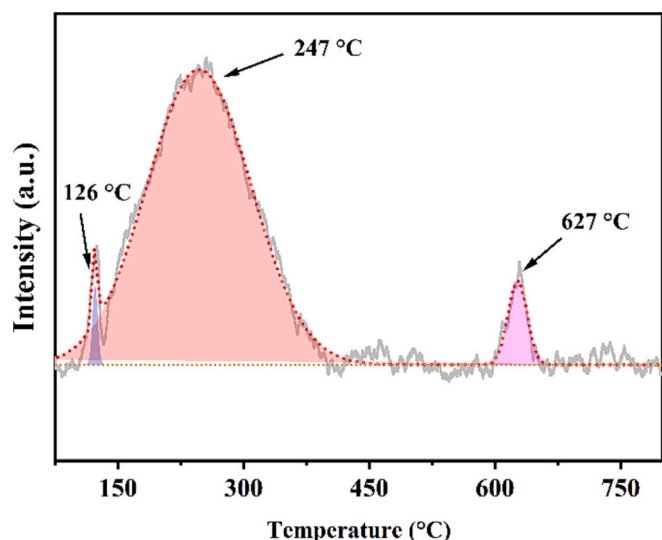


Fig. 6. CO<sub>2</sub>-TPD profiles and Lorentz model fitting curve of MFC-900 sample.

MFC-900 was prepared at a suitable carbonization temperature, which gives it more active sites and more suitable porosity for strong CO<sub>2</sub> interaction, but the weak interaction with N<sub>2</sub>. Moreover, the CO<sub>2</sub>/N<sub>2</sub> selectivity of the MFC materials also varies with adsorption temperature. As the temperature increases, the decrease in CO<sub>2</sub> adsorption amount is smaller than the decrease in N<sub>2</sub> adsorption amount, so the selectivity shows a trend of first increasing and then decreasing. This is determined by the strong interaction and structural characteristics of MFC and CO<sub>2</sub>. Furthermore, the CO<sub>2</sub> capture performance of MFC-900 was investigated by measuring the breakthrough curves of CO<sub>2</sub>/N<sub>2</sub> mixed gas through the column breakthrough experiment. Fig. S7 shows the different breakthrough behaviors of MFC-900 when it adsorbs CO<sub>2</sub>/N<sub>2</sub> mixed gas (15/85 vol%) at 30 °C. The breakthrough curves of CO<sub>2</sub> start at 10–15 min g<sup>-1</sup> and then increased slowly, reach a 50 min adsorption plateau at 80 min g<sup>-1</sup>, and finally ends at 200–210 min g<sup>-1</sup>. In comparison, the breakthrough of N<sub>2</sub> was much faster and complete within 20 min g<sup>-1</sup>. These results indicate that MFC-900 can selectively adsorb CO<sub>2</sub> from mixed gas.

### 3.4. Catalytic evaluation of CO<sub>2</sub> conversion

The cycloaddition reaction of CO<sub>2</sub> with SO is a promising way to convert CO<sub>2</sub> into high-value cyclic carbonates. In this study, we used the prepared MFC materials as catalysts for this reaction. The catalytic performance of different MFC materials are evaluated by product yield under different conditions, as shown in Table 3. It is found that the product yield increases from 62% to 97% as the reaction pressure increased from 4 bar to 6 bar. Therefore, the pressure of 6 bar is selected as the optimal reaction condition for further study. The significant differences in catalytic activity appear for MFC-800, MFC-900 and MFC-1000, which means that higher carbonization temperature would improve the catalytic performance of MFC materials. In contrast, single-component TBAB is almost inert to the cycloaddition reaction, indicating that MFC materials effectively enhanced the activation of the substrate in this reaction. Additionally, adsorption and conversion data of MFC materials show a significant correlation between the total nitrogen content, especially N-5 and N-6, and the CO<sub>2</sub> capture and conversion performance of MFC materials. In particular, the N-5/N-6 ratio seems to directly influence the adsorption efficiency and catalytic activity of the MFC materials. However, even MFC materials with a large specific surface area can exhibit poor CO<sub>2</sub> capture and conversion if the nitrogen content is insufficient or the distribution of nitrogen species is poor. To conclude, nitrogen species and their content are crucial factors for CO<sub>2</sub> capture and conversion, while the specific surface area of the catalyst provides the necessary structural support for these processes. Based on these results, it is inferred that MFC-900 could effectively activate CO<sub>2</sub>, and thus accelerate the reaction efficiency of the cycloaddition reaction.

In order to evaluate the application potential of the optimal catalyst (MFC-900), a series of cycloaddition reactions were carried out between CO<sub>2</sub> and various epoxides. Five representative epoxides were employed as substrates and performed the cycloaddition reaction under the same conditions as before. The product yield and selectivity were detected by GC and summarized in Table 4. It is found that MFC-900 could efficiently catalyze the cycloaddition of various epoxides with CO<sub>2</sub> into corresponding cyclic carbonates with high yield and selectivity. Surprisingly, these findings demonstrate MFC materials have excellent catalytic performance and broad application prospects in the field of CO<sub>2</sub> conversion. Finally, the catalytic activity of the MFC-900 material was compared with that of other similar porous materials, and the comparison are results listed in Table S5. The results indicate that the MFC-900 material has good catalytic activity, meaning it has the potential to effectively convert waste carbon into working carbon.

The elucidation of the reaction mechanism is crucial for revealing the chemical reaction process at the molecular level. Therefore, based on the previous literature [8,33,50] and the experimental data obtained in this

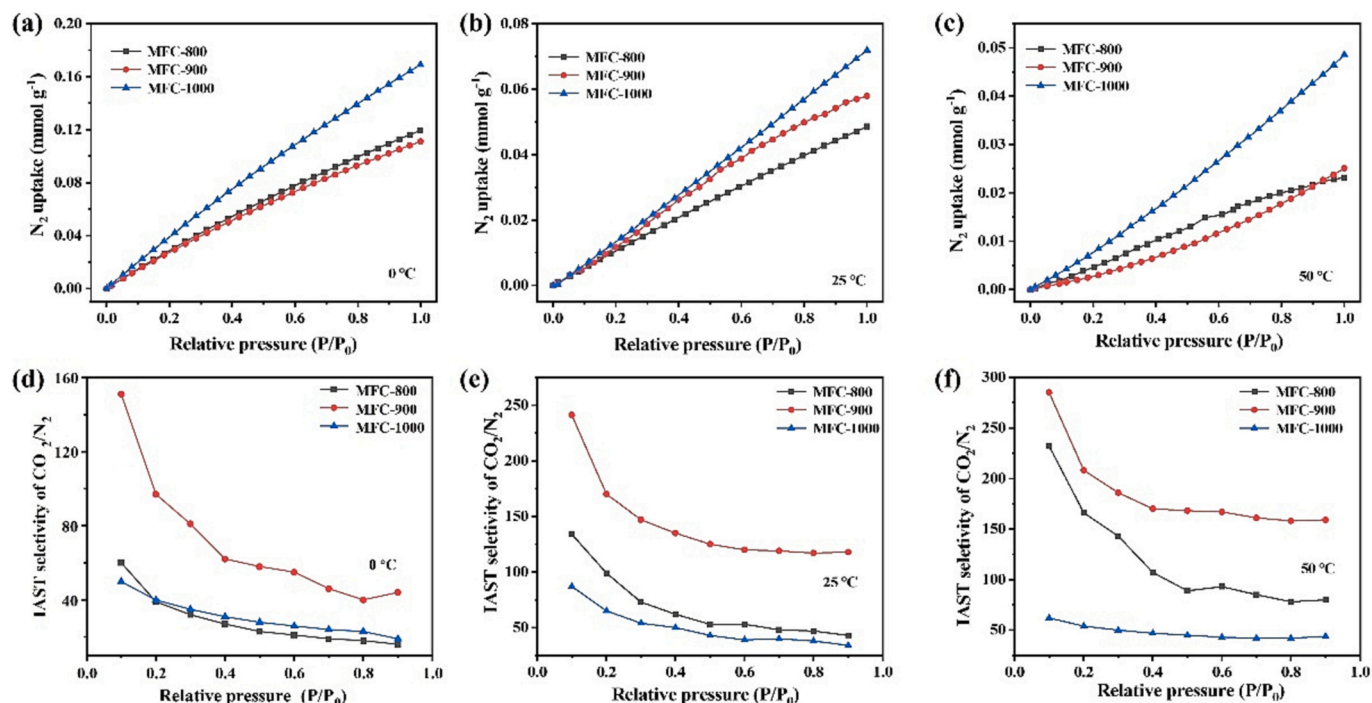


Fig. 7. (a-c) N<sub>2</sub> capture isotherms of MFC-800, MFC-900 and MFC-1000 samples at 1 bar 50 °C, (d-f) IAST selectivities of MFC-800, MFC-900 and MFC-1000 samples for CO<sub>2</sub>/N<sub>2</sub> at 25 °C.

Table 4

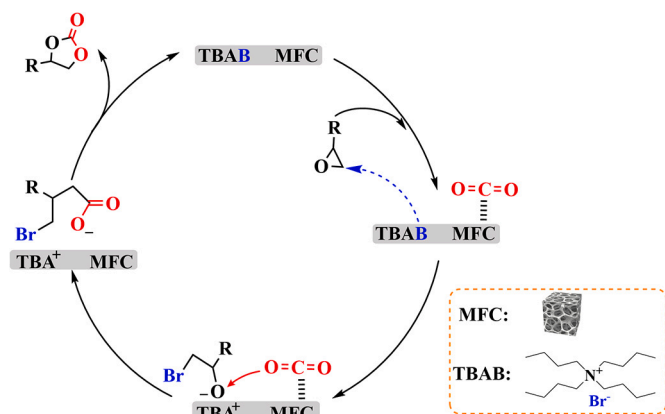
Catalytic activities of various epoxides with CO<sub>2</sub> at 6 bar<sup>a</sup>.

Entry	Substrate	Product	Selectivity (%)	Yield (%)
1			99%	99%
2			99%	97%
3			99%	99%
4			99%	99%
5			99%	97%
6			99%	99%

<sup>a</sup> Reaction condition: epoxides (2 mmol), MFC-900 (20 mg), TBAB (20 mg), 110 °C, 2 h.

work, a possible mechanism for the CO<sub>2</sub> cycloaddition reaction catalyzed by MFC and co-catalyst TBAB is proposed, as shown in Scheme 2. The first step of this reaction involves the attack of nucleophiles on the β-carbon of the epoxides, which leads to the breaks of the C—O bond in the three-membered ring. This process forms intermediates of bromoalkoxides with Br<sup>-</sup> ions, which remains relatively stable with the TBA<sup>+</sup> through the electrostatic interaction of the cation and anion.

Meanwhile, the active sites of the MFC catalysts efficiently activate the CO<sub>2</sub> molecules, which provide the basis for the subsequent cycloaddition of CO<sub>2</sub> and bromoalkoxides. Then, the activated CO<sub>2</sub> is inserted into the bromoalkoxides, and forms alkyl carbonate anions. These intermediates are converted into cyclic carbonates. Upon completion of the reaction, the MFC and TBAB are regenerated and continue to synergistically catalyze the subsequent cycloaddition reactions.



**Scheme 2.** Possible mechanism of the MFC materials catalyzed cycloaddition of CO<sub>2</sub> and epoxides.

The application potential of the MFC-900 material as a CO<sub>2</sub> adsorbent was also evaluated, which was carried out 0 °C and 1 bar, with desorption conditions of 120 °C and ~0.1 kPa, and a degassing time of 2 h. Fig. 8a shows the CO<sub>2</sub> capture of the MFC-900 material at the number of cycles. The results demonstrate that the MFC-900 material has high capture stability and reversibility, as its CO<sub>2</sub> capture capacity only drops slightly from 5.05 mmol g<sup>-1</sup> in the fresh sample to 4.97 mmol g<sup>-1</sup> in the fifth cycle. Fig. 8b illustrates that the MFC catalyst still maintains an SC product yield of >96% after five consecutive cycles, indicating its good stability and recyclability. The MFC catalyst can effectively catalyze the cycloaddition of CO<sub>2</sub> with SO to generate SC as the only product. This provides a highly efficient, low-cost and eco-friendly strategy for the

CCU field.

FT-IR analysis of the cycled and fresh samples (Fig. 8c) shows that MFC-900 material structure is stable. The infrared spectra of the cycled sample are consistent with that of the fresh sample, indicating that there are no significant changes or peak disappearances, which suggests structural stability. Moreover, the recycled MFC-900 material exhibits a similar crystal structure to that of the fresh MFC-900, as shown in Fig. 8d. This indicates that the MFC-900 material did not undergo any major structural changes during the cycling experiments. Therefore, MFC-900 material has good cyclic performance and structural stability, and is expected to be an efficient CO<sub>2</sub> adsorbent in the industrial field.

#### 4. Conclusion

In summary, we successfully convert the waste foam into multi-functional hollow porous materials demonstrating excellent CO<sub>2</sub> capture and conversion performance. MFC materials are featured by high nitrogen content and unique hollow branched fiber structures. These features are proven especially beneficial for CO<sub>2</sub> capture and conversion applications. The MFC-900 material is particularly notable for its CO<sub>2</sub> capture capacity of 5.05/1.37 mmol g<sup>-1</sup> at 1 bar and 0/50 °C conditions, and it has excellent catalytic activity for CO<sub>2</sub> cycloaddition. Impressively, the cycloaddition reaction yields of various epoxides reach 97–99%. The robustness of these materials further demonstrates their ability to maintain performance over multiple adsorption/desorption and reaction cycles, indicating great potential for practical applications in CO<sub>2</sub> capture and conversion processes. Therefore, the development of MFC materials from waste foam provides an exciting and eco-friendly solution for CO<sub>2</sub> capture and conversion, while it offers a promising approach for both waste management and environmental sustainability at the same time.

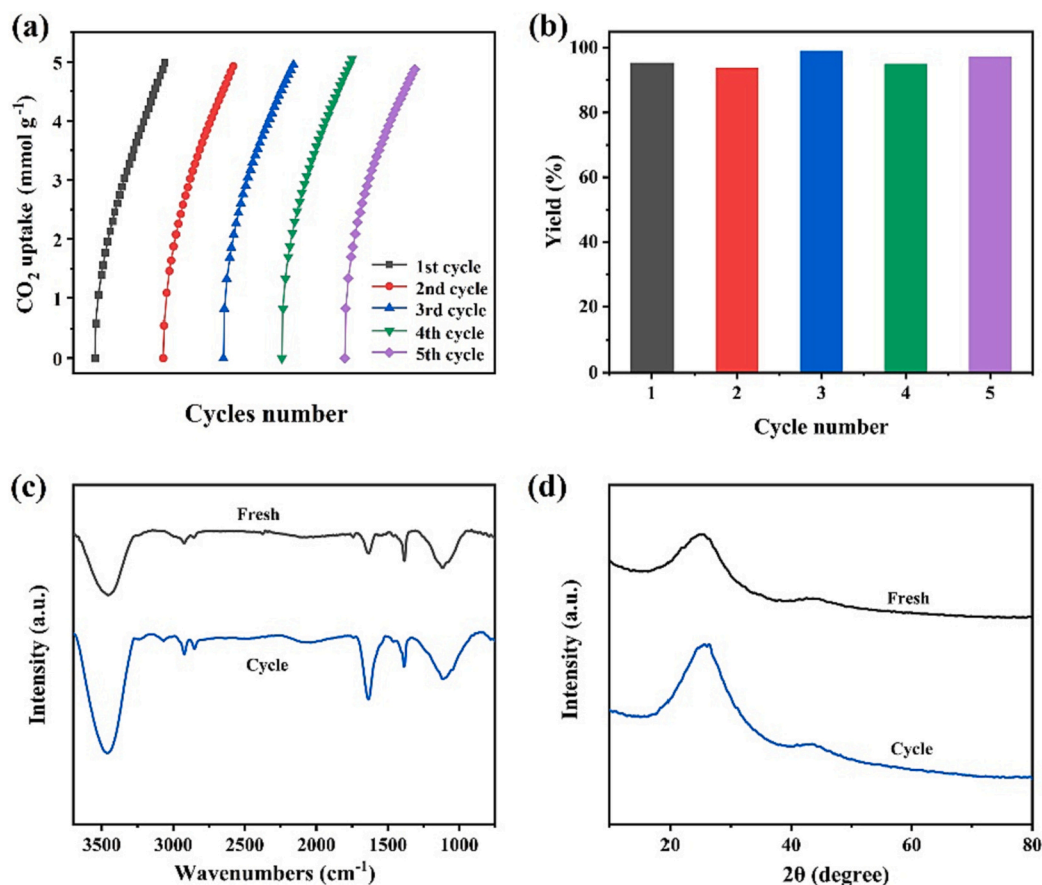


**Fig. 8.** Reusability of MFC-900 sample for (a) CO<sub>2</sub> capture and (b) conversion, (c) FT-IR and (d) XRD of fresh and recycled MFC-900 sample.

## CRedit authorship contribution statement

**Ling Shi:** Visualization, Investigation, Formal analysis. **Ke-Yi Liao:** Investigation, Data curation. **Yu-Hua Dong:** Investigation, Data curation. **Yi-An Wang:** Methodology. **Yan Zhou:** Validation. **Xiu-Guang Yi:** Validation. **Ming-Shuai Sun:** Validation, Methodology. **Wei Hui:** Writing – original draft, Supervision, Funding acquisition, Writing – review & editing. **Duan-Jian Tao:** Supervision, Resources, Funding acquisition, Writing – review & editing.

## Declaration of competing interest

The authors declare that they have no known competing financial interests or personal relationships that could have appeared to influence the work reported in this paper.

## Data availability

Data will be made available on request.

## Acknowledgments

We thank the National Natural Science Foundations of China (22378178, 22168018) and the PhD Start-up Fund of the Natural Science Foundation of Jinggangshan University (JZB2320).

## Appendix A. Supplementary data

Supplementary data to this article can be found online at <https://doi.org/10.1016/j.susmat.2024.e00880>.

## References

- [1] E.S. Sanz-Pérez, C.R. Murdock, S.A. Didas, C.W. Jones, Direct capture of CO<sub>2</sub> from ambient air, *Chem. Rev.* 116 (19) (2016) 11840–11876.
- [2] K. Zhang, D. Guo, X. Wang, Y. Qin, L. Hu, Y. Zhang, R. Zou, S. Gao, Sustainable CO<sub>2</sub> management through integrated CO<sub>2</sub> capture and conversion, *J. CO<sub>2</sub> Utilizat.* 72 (2023) 102493.
- [3] X. Shao, Y. Zhang, X. Miao, W. Wang, Z. Liu, Q. Liu, T. Zhang, J. Ji, X. Ji, Renewable N-doped microporous carbons from walnut shells for CO<sub>2</sub> capture and conversion, *Sustain. Energ. & Fuels* 5 (18) (2021) 4701–4709.
- [4] L. Jiang, A. Gonzalez-Diaz, J. Ling-Chin, A.P. Roskilly, A.J. Smallbone, Post-combustion CO<sub>2</sub> capture from a natural gas combined cycle power plant using activated carbon adsorption, *Appl. Energy* 245 (2019) 1–15.
- [5] L. Liu, S. Jayakumar, J. Chen, L. Tao, H. Li, Q. Yang, C. Li, Synthesis of bifunctional porphyrin polymers for catalytic conversion of dilute CO<sub>2</sub> to cyclic carbonates, *ACS Appl. Mater. Interfaces* 13 (25) (2021) 29522–29531.
- [6] S. Samanta, R. Srivastava, Catalytic conversion of CO<sub>2</sub> to chemicals and fuels: the collective thermocatalytic/photocatalytic/electrocatalytic approach with graphitic carbon nitride, *Mater. Adv.* 1 (6) (2020) 1506–1545.
- [7] A. Rehman, F. Saleem, F. Javed, A. Ikhtlaq, S.W. Ahmad, A. Harvey, Recent advances in the synthesis of cyclic carbonates via CO<sub>2</sub> cycloaddition to epoxides, *J. Environ. Chem. Eng.* 9 (2) (2021) 105113.
- [8] W. Hui, X.-Y. Xu, F.-F. Mao, L. Shi, H.-J. Wang, N/O-rich multilayered ultramicroporous carbon for highly efficient capture and conversion of CO<sub>2</sub> under atmospheric conditions, *Sustain. Energy Fuels* 6 (13) (2022) 3208–3219.
- [9] J.E. Rainbolt, P.K. Koech, C.R. Yonker, F. Zheng, D. Main, M.L. Weaver, J. C. Linehan, D.J. Heldebrant, Anhydrous tertiary alkanolamines as hybrid chemical and physical CO<sub>2</sub> capture reagents with pressure-swing regeneration, *Energy Environ. Sci.* 4 (2) (2011) 480–484.
- [10] J. Wei, Y. Ma, Z. Qin, Z. Jin, Y. Jin, L. Yang, L. Yao, W. Jiang, Y. Deng, Y. Huang, et al., Membrane fabricated via a facile non-solvent induced microstructure rearrangement with superior CO<sub>2</sub> separation performances, *Sep. Purif. Technol.* 320 (2023) 124182.
- [11] O.T. Qazvini, R. Babarao, S.G. Telfer, Selective capture of carbon dioxide from hydrocarbons using a metal-organic framework, *Nat. Commun.* 12 (1) (2021) 197.
- [12] T. Lu, C. Ma, M. Demir, Q. Yu, P. Aghamohammadi, L. Wang, X. Hu, One-pot synthesis of potassium benzoate-derived porous carbon for CO<sub>2</sub> capture and supercapacitor application, *Sep. Purif. Technol.* 301 (2022) 122053.
- [13] J. Bai, J. Huang, Q. Jiang, W. Jiang, M. Demir, M. Kilic, B.N. Altay, L. Wang, X. Hu, Synthesis and characterization of polyphenylene sulfide resin-derived S-doped porous carbons for efficient CO<sub>2</sub> capture, *Colloids Surf. A Physicochem. Eng. Asp.* 674 (2023) 131916.
- [14] G.T. Rochelle, Amine scrubbing for CO<sub>2</sub> capture, *Science* 325 (5948) (2009) 1652–1654.
- [15] X. Liu, Y. Zhou, C.-L. Wang, Y. Liu, D.-J. Tao, Solvent-free self-assembly synthesis of N-doped ordered mesoporous carbons as effective and bifunctional materials for CO<sub>2</sub> capture and oxygen reduction reaction, *Chem. Eng. J.* 427 (2022) 130878.
- [16] E. Favre, Membrane processes and postcombustion carbon dioxide capture: challenges and prospects, *Chem. Eng. J.* 171 (3) (2011) 782–793.
- [17] J. Xiao, X. Yuan, T.C. Zhang, L. Ouyang, S. Yuan, Nitrogen-doped porous carbon for excellent CO<sub>2</sub> capture: a novel method for preparation and performance evaluation, *Sep. Purif. Technol.* 298 (2022) 121602.
- [18] K. Sumida, D.L. Rogow, J.A. Mason, T.M. McDonald, E.D. Bloch, Z.R. Herm, T.-H. Bae, J.R. Long, Carbon Dioxide Capture in Metal–Organic Frameworks, *Chem. Rev.* 112 (2) (2012) 724–781.
- [19] W. Hui, F.-F. Mao, X. Wang, X.-Y. Xu, H.-J. Wang, Enhanced capture of waste and diluted CO<sub>2</sub> by N/O-rich multilayered ultramicropores bio-carbon composites materials, *Composit. Communicat.* 28 (2021) 100961.
- [20] J. Singh, S. Basu, H. Bhunia, CO<sub>2</sub> capture by modified porous carbon adsorbents: effect of various activating agents, *J. Taiwan Inst. Chem. Eng.* 102 (2019) 438–447.
- [21] J. Bai, J. Shao, Q. Yu, M. Demir, B. Nazli Altay, T. Muhammad Ali, Y. Jiang, L. Wang, X. Hu, Sulfur-doped porous carbon adsorbent: a promising solution for effective and selective CO<sub>2</sub> capture, *Chem. Eng. J.* 479 (2024) 147667.
- [22] W. Tu, Y. Zhou, Z. Zou, Photocatalytic conversion of CO<sub>2</sub> into renewable hydrocarbon fuels: state-of-the-art accomplishment, challenges, and prospects, *Adv. Mater.* 26 (27) (2014) 4607–4626.
- [23] R.N. Compton, P.W. Reinhardt, C.D. Cooper, Collisional ionization of Na, K, and Cs by CO<sub>2</sub>, COS, and CS<sub>2</sub>: molecular electron affinities, *J. Chem. Phys.* 63 (9) (2008) 3821–3827.
- [24] J. Lee, D.C. Sorescu, X. Deng, Electron-induced dissociation of CO<sub>2</sub> on TiO<sub>2</sub>(110), *J. Am. Chem. Soc.* 133 (26) (2011) 10066–10069.
- [25] E. Karamian, S. Sharifnia, On the general mechanism of photocatalytic reduction of CO<sub>2</sub>, *J. CO<sub>2</sub> Utilizat.* 16 (2016) 194–203.
- [26] W.D. Jones, Carbon capture and conversion, *J. Am. Chem. Soc.* 142 (11) (2020) 4955–4957.
- [27] Y. Li, B. Zou, C. Hu, M. Cao, Nitrogen-doped porous carbon nanofiber webs for efficient CO<sub>2</sub> capture and conversion, *Carbon* 99 (2016) 79–89.
- [28] F. Nocito, A. Dibenedetto, Atmospheric CO<sub>2</sub> mitigation technologies: carbon capture utilization and storage, *Curr. Opin. Green Sustain. Chem.* 21 (2020) 34–43.
- [29] H.N. Catherine, Z.-T. Liu, C.-Y. Lin, P.-W. Chung, S. Tsunekawa, S.D. Lin, M. Yoshida, C. Hu, Understanding the intermediates and carbon dioxide adsorption of potassium chloride-incorporated graphitic carbon nitride with tailoring melamine and urea as precursors, *J. Colloid Interface Sci.* 633 (2023) 598–607.
- [30] D.-J. Tao, F.-F. Mao, J.-J. Luo, Y. Zhou, Z.-M. Li, L. Zhang, Mesoporous N-doped carbon derived from tea waste for high-performance CO<sub>2</sub> capture and conversion, *Mater. Today Communicat.* 22 (2020) 100849.
- [31] H. Wang, X. Li, Z. Cui, Z. Fu, L. Yang, G. Liu, M. Li, Coffee grounds derived N enriched microporous activated carbons: efficient adsorbent for post-combustion CO<sub>2</sub> capture and conversion, *J. Colloid Interface Sci.* 578 (2020) 491–499.
- [32] F. Yang, J. Wang, L. Liu, P. Zhang, W. Yu, Q. Deng, Z. Zeng, S. Deng, Synthesis of porous carbons with high N-content from shrimp shells for efficient CO<sub>2</sub>-capture and gas separation, *ACS Sustain. Chem. Eng.* 6 (11) (2018) 15550–15559.
- [33] D. Polidoro, A. Perosa, E. Rodríguez-Castellón, P. Canton, L. Castoldi, D. Rodríguez-Padrón, M. Selva, Metal-free N-doped carbons for solvent-less CO<sub>2</sub> fixation reactions: a shrimp Shell valorization opportunity, *ACS Sustain. Chem. Eng.* 10 (41) (2022) 13835–13848.
- [34] L. Shen, H. Zhang, Y. Lei, Y. Chen, M. Liang, H. Zou, Hierarchical pore structure based on cellulose nanofiber/melamine composite foam with enhanced sound absorption performance, *Carbohydr. Polym.* 255 (2021) 117405.
- [35] N. Zheng, C. Zhang, R. Fan, Z. Sun, Melamine foam-based shape-stable phase change composites enhanced by aluminum nitride for thermal management of lithium-ion batteries, *J. Energ. Storag.* 52 (2022) 105052.
- [36] M.E. Casco, M. Martínez-Escandell, J. Silvestre-Albero, F. Rodríguez-Reinoso, Effect of the porous structure in carbon materials for CO<sub>2</sub> capture at atmospheric and high-pressure, *Carbon* 67 (2014) 230–235.
- [37] W. Hui, L. Shi, X.-Y. Xu, H.-J. Wang, M.-S. Sun, D.-J. Tao, Rapid and effective cycloaddition of environmentally diluted CO<sub>2</sub> catalyzed by hierarchical porous ionic carbon at atmospheric conditions, *J. Environ. Chem. Eng.* 11 (2) (2023) 109458.
- [38] Y. Shen, Z. Lin, J. Wei, Y. Xu, Y. Wan, T. Zhao, X. Zeng, Y. Hu, R. Sun, Facile synthesis of ultra-lightweight silver/reduced graphene oxide (rGO) coated carbonized-melamine foams with high electromagnetic interference shielding effectiveness and high absorption coefficient, *Carbon* 186 (2022) 9–18.
- [39] N.F. Attia, M. Jung, J. Park, H. Jang, K. Lee, H. Oh, Flexible nanoporous activated carbon cloth for achieving high H<sub>2</sub>, CH<sub>4</sub>, and CO<sub>2</sub> storage capacities and selective CO<sub>2</sub>/CH<sub>4</sub> separation, *Chem. Eng. J.* 379 (2020) 122367.
- [40] J. Luo, Y. Chen, H. Huang, R. Ma, N. Ma, F. Yan, J. Xu, J. Zhang, J. Chen, S. Sun, Microwave-coordinated KOH directionally modulated N/O co-doped porous biochar from Enteromorpha and its structure–effect relationships in efficient CO<sub>2</sub> capture, *Chem. Eng. J.* 473 (2023) 145279.
- [41] U. Kamran, K.Y. Rhee, S.-Y. Lee, S.-J. Park, Solvent-free conversion of cucumber peels to N-doped microporous carbons for efficient CO<sub>2</sub> capture performance, *J. Clean. Prod.* 369 (2022) 133367.
- [42] M.A. Islam, M.A. Kalam, M.R. Khan, Reactive gas solubility in water: an empirical relation, *Ind. Eng. Chem. Res.* 39 (7) (2000) 2627–2630.
- [43] G. Singh, I.S. Ismail, C. Bilen, D. Shanbhag, C.I. Sathish, K. Ramadass, A. Vinu, A facile synthesis of activated porous carbon spheres from d-glucose using a non-corrosive activating agent for efficient carbon dioxide capture, *Appl. Energy* 255 (2019) 113831.

- [44] M. Mihaylov, K. Chakarova, S. Andonova, N. Drenchev, E. Ivanova, E.A. Pidko, A. Sabetghadam, B. Seoane, J. Gascon, F. Kapteijn, et al., Adsorption of CO<sub>2</sub> on MIL-53(Al): FTIR evidence of the formation of dimeric CO<sub>2</sub> species, *Chem. Commun.* 52 (7) (2016) 1494–1497.
- [45] S.O. Adio, S.A. Ganiyu, M. Usman, I. Abdulazeez, K. Alhooshani, Facile and efficient nitrogen modified porous carbon derived from sugarcane bagasse for CO<sub>2</sub> capture: experimental and DFT investigation of nitrogen atoms on carbon frameworks, *Chem. Eng. J.* 382 (2020) 122964.
- [46] J. Serafin, J. Sreńscek-Nazzal, A. Kamińska, O. Paszkiewicz, B. Michalkiewicz, Management of surgical mask waste to activated carbons for CO<sub>2</sub> capture, *J. CO<sub>2</sub> Utilizat.* 59 (2022) 101970.
- [47] X. Zhang, S. Zhang, H. Yang, J. Shao, Y. Chen, Y. Feng, X. Wang, H. Chen, Effects of hydrofluoric acid pre-deashing of rice husk on physicochemical properties and CO<sub>2</sub> adsorption performance of nitrogen-enriched biochar, *Energy* 91 (2015) 903–910.
- [48] M.-J. Kim, S.W. Choi, H. Kim, S. Mun, K.B. Lee, Simple synthesis of spent coffee ground-based microporous carbons using K<sub>2</sub>CO<sub>3</sub> as an activation agent and their application to CO<sub>2</sub> capture, *Chem. Eng. J.* 397 (2020) 125404.
- [49] X. Shao, Z. Feng, R. Xue, C. Ma, W. Wang, X. Peng, D. Cao, Adsorption of CO<sub>2</sub>, CH<sub>4</sub>, CO<sub>2</sub>/N<sub>2</sub> and CO<sub>2</sub>/CH<sub>4</sub> in novel activated carbon beads: preparation, measurements and simulation, *AIChE J.* 57 (11) (2011) 3042–3051.
- [50] A. Giri, N.N. Patil, A. Patra, Porous noria polymer: a cage-to-network approach toward a robust catalyst for CO<sub>2</sub> fixation and nitroarene reduction, *Chem. Commun.* 57 (36) (2021) 4404–4407.